JCTC Journal of Chemical Theory and Computation

pubs.acs.org/JCTC Article

Newton-X Platform: New Software Developments for Surface Hopping and Nuclear Ensembles

Mario Barbatti,* Mattia Bondanza, Rachel Crespo-Otero, Baptiste Demoulin, Pavlo O. Dral, Giovanni Granucci, Fábris Kossoski, Hans Lischka, Benedetta Mennucci, Saikat Mukherjee, Marek Pederzoli, Maurizio Persico, Max Pinheiro Jr, Jiří Pittner, Felix Plasser, Eduarda Sangiogo Gil, and Ljiljana Stojanovic

Cite This: *J. Chem. Theory Comput.* 2022, 18, 6851−6865 Read Online

ACCESS | Metrics & More | Article Recommendations

ABSTRACT: Newton-X is an open-source computational platform to perform nonadiabatic molecular dynamics based on surface hopping and spectrum simulations using the nuclear ensemble approach. Both are among the most common methodologies in computational chemistry for photophysical and photochemical investigations. This paper describes the main features of these methods and how they are implemented in Newton-X. It emphasizes the newest developments, including zero-point-energy leakage correction, dynamics on complex-valued potential energy surfaces, dynamics induced by incoherent light, dynamics based on machine-learning potentials, exciton dynamics of multiple chromophores, and supervised and unsupervised machine learning techniques. Newton-X is interfaced with several third-party quantum-chemistry programs, spanning a broad spectrum of electronic structure methods.

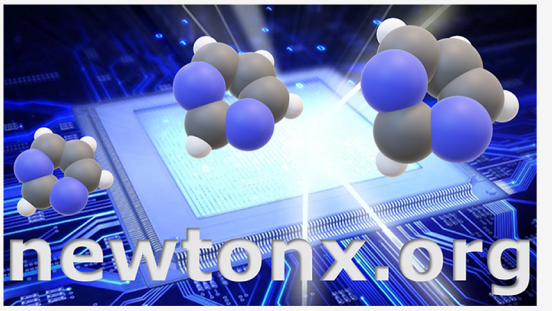

1. INTRODUCTION

Incoherent techniques for treating excited states have been the primary driver for the surge of photoexcitation studies in the last couple of decades. These techniques approximate the nuclear part of the molecular wave function as ensembles of classical systems, with each element independent of the others. Two such techniques, the trajectory surface hopping (TSH; all acronyms are defined at the end of this paper) for nonadiabatic dynamics and the nuclear ensemble approach (NEA) for spectrum simulations, are the workhorse methods for computational photochemistry.[1−3] Newton-X (www.newtonx.org) is an open-source software platform tailored for these two types of simulations.

The Newton-X development started in 2005 based on surface hopping codes developed by Granucci et al.[4] The first paper describing Newton-X (version 0.13) was published in 2007.[5] Seven years later, a second paper reported the new developments in the program, at that point, still in version 1.4.[6] Since then, other 8 years have passed, and Newton-X has branched into four stand-alone software packages (Figure 1): Initcond for nuclear ensemble simulations, Newton-X *classical series* (CS), Newton-X *new series* (NS), both for dynamics, and Ulamdyn for data analysis. Now that the Newton-X CS has reached version 3, it is an adequate time to synthesize the software's status in a new publication, crediting many new coauthors who joined the software development.

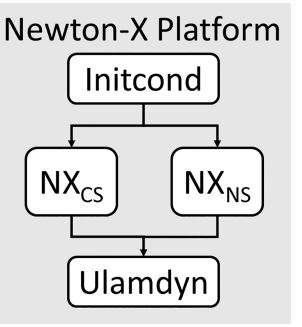

Figure 1. Newton-X platform. Newton-X is branched into four stand-alone programs: Initcond for nuclear ensembles, spectra, and initial conditions; Newton-X CS and NS for dynamics; and Ulamdyn for data analysis, including unsupervised ML.

This paper focuses on Initcond and Newton-X CS. However, whenever we mention Newton-X without specifying

Received: August 4, 2022
Published: October 4, 2022

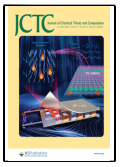

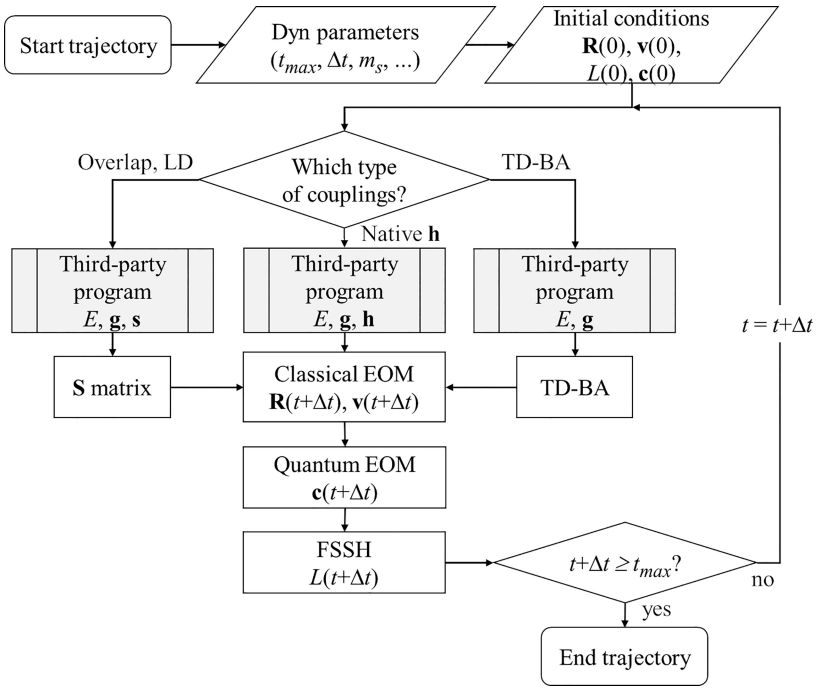

Figure 2. Flowchart of nonadiabatic dynamics in Newton-X CS. To run a single trajectory, the user should provide dynamics parameters defining the methods to be used and the initial conditions, including the molecular initial state L. Newton-X calls third-party quantum-chemical programs to compute electronic energies (E), energy gradients (**g**), and, optionally, either nonadiabatic coupling vectors (**h**) or atomic orbital overlaps between different time steps (**s**). The latter is employed to build the wave function overlap matrix **S** for either time derivative couplings or LD. All this information comes together to propagate classical and quantum EOM in one time step. The FSSH is used to determine the electronic state L for the new time step.

the series, the feature in question should be valid for both CS and NS. Newton-X NS's core features are discussed in Section 7. Ulamdyn is introduced in Section 6.3.

When Newton-X was first released in 2007, it was one of the first publicly available software for surface hopping and nuclear ensembles using quantum-chemical methods. (A few earlier surface hopping codes were available, like those implemented in ANT,[7] CPMD,[8] or MOPAC.[4]) Since then, many other options have appeared,[9−19] each excelling in specific niches. Newton-X remains relevant by providing a complete set of tools for all steps of the nonadiabatic dynamics research, from spectrum simulations to advanced data analysis. Thus, it became a platform for external developments,[20−24] which are eventually included in the public version. Moreover, Newton-X counts on an active developers' basis, implementing new methodologies to extend the domain of applicability of standard approaches.

In recent years, Newton-X became the host of novel methods for nonadiabatic couplings without wave functions,[25] zero-point-energy (ZPE) leakage corrections,[26] and nonadiabatic dynamics induced by incoherent light,[27] on complex-valued potential energy surfaces,[28] and including multiple chromophores.[29] All these features, together with interfaces to numerous third-party program spanning methods from MRCI to machine learning (ML) potentials, make Newton-X one of the richest software platforms for mixed quantum-classical simulations. This paper reviews the basic concepts underlying TSH and NEA and all these novel developments, delivering an integrated overview of the Newton-X capabilities.

2. PROGRAM ARCHITECTURE

Newton-X is primarily focused on atomistic simulations, meaning that molecules are described as nuclei and electrons treated within the Born−Oppenheimer approximation, with nonadiabatic effects added as a correction. In principle, neither dynamics nor nuclear ensembles require model Hamiltonians or precomputed, fitted potential energy surfaces. The programs are tailored to evaluate on the fly the electronic properties at specific nuclear coordinates determined by dynamics or probability distribution functions.

The electronic structure calculations are carried out by third-party computational chemistry programs interfaced with Newton-X. Newton-X CS uses Perl scripts to call such interfaces, execute the third-party programs, read their outputs, and use their results to propagate dynamics, compute nonadiabatic couplings, and simulate spectra. The numerical integration of the classical and quantum equations of motion (EOM), the surface hopping algorithm, and the Wigner sampling are executed by Fortran codes. The interfaces to third-party programs are defined in a shared Perl dictionary (hash), which controls default and execution parameters. The currently available interfaces are discussed in Section 5. The development of an interface to a new third-party program consists of defining its primary operation in the dictionary and preparing scripts to execute and read the outputs of that program.

3. SURFACE HOPPING

The primary nonadiabatic dynamics method implemented in Newton-X is the decoherence-corrected fewest-switches surface hopping (DC-FSSH) approach. In this section, we review the main aspects and variants of the method as implemented in

https://doi.org/10.1021/acs.jctc.2c00804
J. Chem. Theory Comput. 2022, 18, 6851−6865

Newton-X CS. The essential software operation is illustrated in Figure 2.

3.1. Classical EOM. The classical positions of the nuclei are determined by integrating Newton's equations with the velocity-Verlet algorithm[30,31] with time step Δt

$$\mathbf{R}(t+\Delta t) = \mathbf{R}(t) + \mathbf{v}(t)\Delta t + \frac{1}{2}\mathbf{a}(t)\Delta t^2$$
$$\mathbf{v}(t+\Delta t) = \mathbf{v}(t) + \frac{1}{2}(\mathbf{a}(t) + \mathbf{a}(t+\Delta t))\Delta t \quad (1)$$

where $\mathbf{R}$ and $\mathbf{v}$ are the Cartesian coordinates and velocities, respectively. The acceleration $\mathbf{a}_\alpha$ of an atom α is obtained from the energy gradient of the adiabatic electronic state L

$$\mathbf{a}_\alpha(t) = -\frac{1}{M_\alpha}\nabla_\alpha E_L(\mathbf{R}(t)) \quad (2)$$

By default, Newton-X trajectories conserve the total energy. Optionally, propagation with a constant temperature can be employed with the Andersen thermostat.[32]

3.2. ZPE Leakage Correction. Newton-X contains a method to correct ZPE leakage in classical trajectories, the local-pair (LP) ZPE correction.[26] The method is tailored for on-the-fly propagation and does not require Hessian matrices, which are too expensive to be tracked during dynamics. LP-ZPE monitors the mean kinetic energy of high-frequency atom pairs instead of the normal modes. If this mean value drops below a threshold, the pair is topped up with energy pumped from other pairs.

The LP-ZPE method is built to have minimum interference in the dynamics, with energy being transferred through instantaneous, fictitious central forces. Thus, it conserves the system's total energy and linear momentum. The angular momentum of the atom pairs is conserved too. The LP-ZPE correction needs only three adjustable parameters independently of the system size. The first parameter describes the period for averaging the parallel component of the kinetic energy of a local pair monitored for ZPE leakage. At the beginning of the dynamics, one should allow the fast-moving bonds (like O−H, for instance) to undergo a few oscillations to obtain a reference of the ZPE value of the local pair. Alternatively, the reference energy can be directly provided, which is useful when dealing with vibrationally excited states. The second parameter dictates how often the correction occurs during the classical propagation. The last parameter controls how much energy leakage is allowed from the reference ZPE value.

An example of the unphysical effects of ZPE leakage is seen in the dynamics of water dimers (Figure 3). A weak interaction binds the dimer in its lowest vibrational state.[33] However, ZPE leaks from the fast OH vibrational modes to the slow intermolecular modes, leading to an artificial dimer dissociation within a few picoseconds during dynamics in the ground state. LP-ZPE inhibits this artifact by continuously monitoring the mean kinetic energy in each OH pair and correcting them when needed.[26] The impact of the LP-ZPE algorithm tends to be tiny. In the water dimer test case, each LP-ZPE application pumped 3 meV on average into a single OH bond and removed 0.26 meV from each donating pair.

3.3. Decoherence-Corrected FSSH. In our implementation of the FSSH,[34] the time-dependent electronic wave function Ansatz is written as[35]

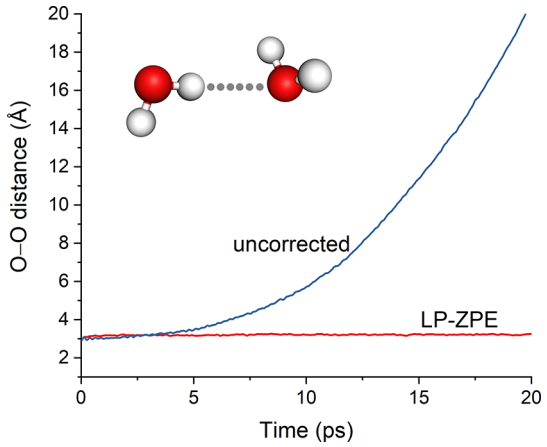

Figure 3. LP-ZPE applied to water dimer. The figure shows the mean value of the O−O distance as a function of time for uncorrected and ZPE-leakage-corrected ground-state dynamics. Uncorrected ground-state dynamics predicts that the dimer should dissociate within a few picoseconds. When the LP-ZPE correction is applied, the dimer does not dissociate. Data from ref 26.

$$|\psi(t)\rangle = \sum_K c_K(t) e^{-i\gamma_K(t)} |K\rangle \quad (3)$$

where $|K\rangle$ are the adiabatic states, and the phase is

$$\gamma_K = \frac{1}{\hbar}\int_0^t E_K(\mathbf{R}(t'))\, dt' \quad (4)$$

E_K is the adiabatic energy computed for the nuclear geometry $\mathbf{R}$. The time-dependent complex-valued coefficients $\mathbf{c}$ of eq 3 are obtained by integrating a local approximation of the Schrödinger equation[36]

$$\frac{dc_J}{dt} = -\sum_{K\neq J} c_K e^{i\gamma_{JK}}\sigma_{JK} \quad (5)$$

where $\gamma_{JK} = \gamma_J - \gamma_K$ and

$$\sigma_{JK} \equiv \langle J|\frac{\partial}{\partial t}K\rangle = \mathbf{v}\cdot\mathbf{h}_{JK} \quad (6)$$

is the time derivative nonadiabatic coupling. In this last equation

$$\mathbf{h}_{JK} \equiv \langle J|\frac{\partial}{\partial \mathbf{R}}K\rangle \quad (7)$$

is the first-order nonadiabatic coupling vector. Either σ_{JK} or $\mathbf{h}_{JK}$ can be used; see Section 3.5.

The classical time step Δt can be divided into m_s substeps, and eq 5 is integrated with a time step $\Delta\tau = \Delta t/m_s$ much smaller than the classical step of eq 1. Several algorithms are available in Newton-X for this integration, and we use the Butcher algorithm[37] by default. Energies, nuclear velocities, and couplings are computed only at the classical steps. For the integration of eq 5, the values of these quantities in each substep are obtained by interpolating between classical steps.

Instead of directly integrating eq 5, the coefficients $\mathbf{c}$ can also be obtained via local diabatization (LD), as discussed in Section 3.4.

Newton-X can correct the overcoherence[38,39] in FSSH either with the simplified decay of mixing[40] (SDM) or with the *overlap-driven decoherence correction* (ODC) approach.[41] In SDM, inspired by Truhlar and co-workers' decay of mixing

https://doi.org/10.1021/acs.jctc.2c00804
J. Chem. Theory Comput. 2022, 18, 6851−6865

method,[42,43] the coefficients **c** are corrected according to eq 17 of ref 40, which assumes that the decoherence time is a function of the energy gap and the nuclear kinetic energy.

The ODC correction is more involved than the SDM. In brief, it attributes a leading frozen Gaussian wave packet to the current state, centered at the classical phase space point. Whenever the hopping probability of another state increases, an ancillary frozen Gaussian wave packet is assigned to this other state. As the trajectory evolves, the ancillary wave packets are propagated too. This propagation is done with a crude approximation based on the classical kinetic energy and energy gaps to avoid additional time overhead. The overlap between the leading wave packet and the ancillary ones is monitored. When this overlap drops below a predefined threshold, the ancillary wave packet is deleted, and its probability is attributed to the current state. Other overlap-based decoherence algorithms are discussed in refs 44 and 45.

Either with the DC-corrected or the uncorrected coefficients **c**, the FSSH hopping probability is

$$P_{L\to J}(t) = \max\left[0, \frac{-2\Delta\tau}{\rho_{LL}(t)}\sigma_{JL}(t)\mathrm{Re}(\rho_{JL}^{*}(t)e^{i\gamma_{JL}(t)})\right] \tag{8}$$

where

$$\rho_{LJ}(t) = c_L(t)c_J^{*}(t) \tag{9}$$

Every time step, a uniform random number r_t is sampled in the [0,1] interval. A hopping from state L to J happens if

$$\sum_{K=1}^{J-1} P_{L\to K} < r_t \le \sum_{K=1}^{J} P_{L\to K} \tag{10}$$

and there is enough kinetic energy to allow energy conservation after hopping over an energy gap ΔE_{LJ}. If this second criterion is not satisfied, the hopping is frustrated, and the trajectory remains on the same surface. However, if the hopping takes place, the nuclear velocity is adjusted to enforce total energy conservation (see Sections II and III of ref 46 for details of the adjustment algorithm).

In Newton-X, this velocity adjustment can be made either in the direction of the nonadiabatic coupling vector (if available) or in any direction in the plane defined by the nonadiabatic coupling and gradient difference vectors. When these vectors are unknown, velocity adjustment is made in the direction of the momentum. This latter choice is not size extensive and may lead to an artificial excess of back hoppings.[47,48] This problem can be avoided by allowing hoppings to upper states only if the energy required is smaller than the nuclear kinetic energy per degree of freedom. The size-extensivity problem is already noticeable for medium-sized molecules. In ref 49, for example, reducing the kinetic energy available for back hopping was imperative to adequately describe the excited-state dynamics of pyrene (26 atoms) after excitation into S_7.

3.4. Local Diabatization. Instead of the direct integration of eq 5, an alternative strategy to perform FSSH is the LD approach,[4,50] which is intended to provide enhanced numerical stability in the case of highly peaked nonadiabatic couplings, including the limiting situation of *trivial*[51] (or *unavoided*[52]) crossings.

In LD, the coefficients **c** are obtained through a unitary transformation

$$\mathbf{c}(t + \Delta t) = \mathbf{T}^{\dagger}e^{-i\mathbf{Z}\Delta t}\mathbf{c}(t) \tag{11}$$

where **T** is an adiabatic-to-diabatic transformation matrix at time $t + \Delta t$. (In LD, $\Delta\tau = \Delta t$.) The diabatic states correspond to the adiabatic ones at the beginning of the integration time step, and the **T** matrix is obtained by Löwdin orthonormalization of the wave function overlap matrix

$$S_{JK}(t + \Delta t) \equiv \langle J(t)|K(t + \Delta t)\rangle \tag{12}$$

The matrix **Z** in eq 11 is obtained by linearly interpolating the diabatic Hamiltonian matrix between t and $t + \Delta t$. Once the coefficients **c** are calculated, they should be corrected for overcoherence using either SDM or ODC, and the hopping probabilities are computed with eq (A.6) of ref 53.

3.5. Nonadiabatic Couplings. If native nonadiabatic coupling vectors **h** are available in the third-party program, Newton-X can use them to propagate the dynamics. Due to the arbitrary sign of the wave functions, the coupling phase is tracked and corrected when necessary. The phase tracking is done by comparing the current coupling to a coupling extrapolated from previous steps. This procedure can distinguish between an arbitrary phase change from a physical sign flip because the extrapolated coupling can change the sign when diabatic characters flip their orders.

For several interfaces, Newton-X allows computing time derivative couplings σ_{JK} with the Hammes−Schiffer/Tully[54] approach

$$\sigma_{JK}(t) \approx \frac{1}{4\Delta t}[3S_{JK}(t) - 3S_{KJ}(t) - S_{JK}(t - \Delta t) + S_{KJ}(t - \Delta t)] \tag{13}$$

where the overlap functions are defined in eq 12. These functions can be obtained with two different methods, the *determinant derivative*[55] (DD) and the *orbital derivative*[56,57] (OD) approaches. In both cases, they depend on the calculations of atomic orbital overlap integrals between different time steps. OD overlap calculations are much faster than calculations of DD overlaps. However, OD overlaps are limited to single excitations, while DD overlaps can deal with any excitation rank. These same overlap functions are used for LD (Section 3.4).

For linear response methods, the electronic wave functions used to compute the overlap are based on Casida's auxiliary multielectron wave functions corresponding to the configuration interaction Ansatz

$$|K\rangle = \sum_{ia} C_{ia}^{K}|ia\rangle \tag{14}$$

where $|ia\rangle$ are Slater determinants with a single excitation from orbital i into orbital a and the linear response coefficients for C_{ia}^{K}.[19,58−60]

3.6. Nonadiabatic Couplings without Wave Functions. For all methods available in Newton-X, nonadiabatic couplings can be calculated with the time-dependent Baeck-An approach[25] (TD-BA), which approximates the time derivative couplings in terms of the energy gaps and their second time derivatives

https://doi.org/10.1021/acs.jctc.2c00804
J. Chem. Theory Comput. 2022, 18, 6851−6865

$$\sigma_{JK} \approx \begin{cases} \dfrac{\mathrm{sgn}(\Delta E_{JK})}{2}\sqrt{\dfrac{1}{\Delta E_{JK}}\dfrac{\mathrm{d}^2\Delta E_{JK}}{\mathrm{d}t^2}} & \text{if} \quad \dfrac{1}{\Delta E_{JK}}\dfrac{\mathrm{d}^2\Delta E_{JK}}{\mathrm{d}t^2} > 0 \\ 0 & \text{if} \quad \dfrac{1}{\Delta E_{JK}}\dfrac{\mathrm{d}^2\Delta E_{JK}}{\mathrm{d}t^2} \le 0 \end{cases} \tag{15}$$

The TD-BA approach does not require wave functions to estimate the coupling, employing only the topographic features of the potential energy surfaces as given during the propagation. Thus, the method can be universally used with any electronic structure for which excited-state dynamics is possible.

Nevertheless, TD-BA does not replace the full coupling calculation and should be reserved for exploratory dynamics, where qualitative results are acceptable. Bearing this warning in mind, ref 25 shows that the nonadiabatic dynamics of ethylene and fulvene (Figure 4) are well described by TD-BA. Good results with the TD-BA approach have also been reported in ref 61.

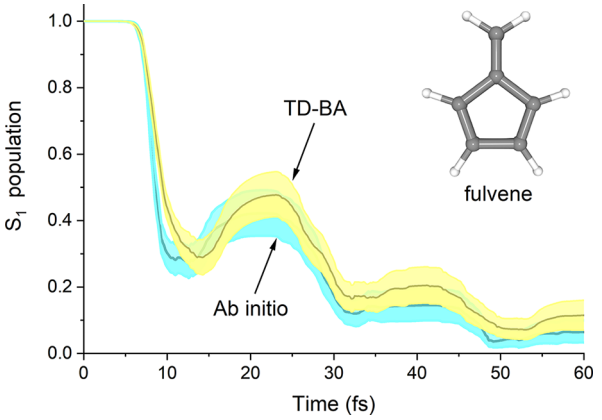

Figure 4. S_1 population of fulvene. Mean population from DC-FSSH dynamics with 200 trajectories in each set. CASSCF(6,6)/6-31G(d) level state-averaged over two states. Integration with 0.1 fs classical time step and 0.005-fs quantum time step. Data from ref 25. The TD-BA set uses TD-BA couplings. The ab initio set uses CASSCF nonadiabatic coupling vectors. In both cases, velocity adjustment after hopping is made in the momentum direction with full kinetic energy. The shaded regions are the margin of errors for a 95% confidence interval sampled with bootstrap through 10,000 repetitions of the 200 trajectories of each dataset. The margins of error are computed with Ulamdyn (see Section 6.3).

3.7. FSSH on Complex-Valued Surfaces.

Complex-valued potentials can be employed to simulate nonreversible processes in which the wave function norm is not conserved. In Newton-X *classical series*, such simulations are done with an FSSH generalization to complex-valued surfaces (CS-FSSH).[28] In this case, the Hamiltonian has an imaginary component, and it is written

$$H = H^R + iH^I \tag{16}$$

With this Hamiltonian, the wave function Ansatz in eq 3 leads to

$$\frac{\mathrm{d}c_J}{\mathrm{d}t} = -c_J\frac{\Gamma_J}{2\hbar} - \sum_{K\neq J} c_K e^{i\gamma_{JK}}\left(\sigma_{JK} + \frac{\Gamma_{JK}}{2\hbar}\right) \tag{17}$$

where

$$\Gamma_{JK} \equiv -2\langle J|H^I|K\rangle$$
$$\Gamma_J \equiv -2\langle J|H^I|J\rangle \tag{18}$$

Unlike the original FSSH, the complex-valued version has a norm-dissipative contribution Γ_J and an additional coupling term Γ_{JK}.

The fewest switches hopping probability is generalized to

$$P_{L\to J}(t) = \max\left[0, \frac{-2\Delta\tau}{\rho_{LL}(t)}\mathrm{Re}\left(\left(\sigma_{JL}(t) - \frac{\Gamma_{JL}(t)}{2\hbar}\right)\rho_{JL}^*(t)e^{i\gamma_{JL}(t)}\right)\right] \tag{19}$$

CS-FSSH can be employed for describing many metastable molecular systems. Examples of such systems are super-excited[62] and core-excited states,[63] and transient anion states that are formed by electron impact, photoexcitation, or bimolecular collisions.[64] All these states are electronically metastable because they may decay by ejecting an electron.

Reference 28 applied CS-FSSH to iodoethene dissociation induced by low-energy electron attachment, unveiling the underlying relaxation mechanisms of the transient anion states. The molecule displays a prototypical π^*/σ^* indirect dissociative electron attachment mechanism, which should also be encountered in biologically relevant halogen-containing molecules. CS-FSSH showed that the electron capture into the π^* orbital promotes C═C stretching and out-of-plane vibrations. It is followed by charge transfer from the double bond into the σ^* orbital at the C−I bond and, finally, the release of the iodide ion, all within only 15 fs. Although this π^*/σ^* mechanism is widely accepted to take place in unsaturated halogenated species,[65] CS-FSSH delivered the first theoretical demonstration of its occurrence.

3.8. Nonadiabatic Dynamics Induced by Incoherent Light.

Usually, in surface hopping simulations, the excitation pulse is supposed to be instantaneous. Thus, dynamics start in the excited state without any explicit pulse description. Nevertheless, the instantaneous pulse hypothesis is not adequate in excitation by thermal (incoherent) light, like solar irradiation.[66] Thermal light is better represented by a continuous field acting on the molecule, slowing transporting electronic density to the excited state. The mixed quantum-classical pulsed ensemble[27] (MQC-PE) method makes it possible to simulate the action of such thermal sources with minimal changes in conventional DC-FSSH. It simulates the incoherent light as an ensemble of pulses, following the Chenu−Brumer approach.[66]

In MQC-PE, the initial state L from where the trajectory should start is sampled with the probability distribution given by the black body radiance at temperature T [see inequality (31)]. The dynamics is carried out using conventional DC-FSSH. After the simulations are finished, ensemble averages are computed by translating the initial time of each trajectory to span the whole illumination window and weighting each trajectory by the field-induced initial-state population [eq 10 of ref 27].

As an example of how the photophysics under incoherent light differs from that induced by short, coherent laser pulses, consider the cis−trans photoisomerization of retinal, studied

https://doi.org/10.1021/acs.jctc.2c00804
J. Chem. Theory Comput. 2022, 18, 6851−6865

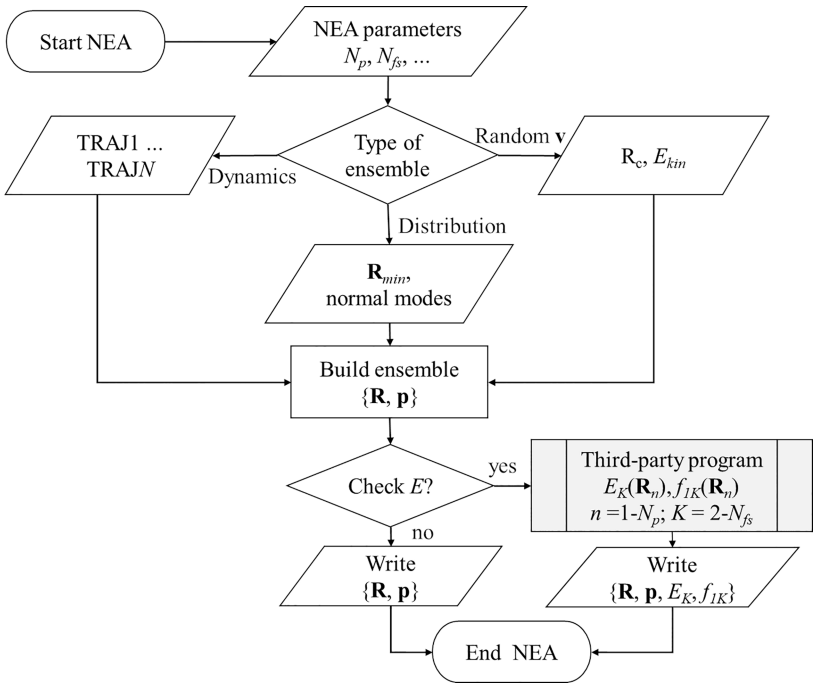

Figure 5. Flowchart of the NEA in Newton-X. After initializing ensemble parameters such as the number of geometries (N_p) and the number of excited states (N_{fs}), an ensemble of Cartesian nuclear geometries ($\mathbf{R}_n$) and momenta ($\mathbf{p}_n$) are built either using probability distributions or picking them from some precomputed dynamics. Random momenta for a fixed geometry can also be created. Optionally, excited-state energies ($E_K(\mathbf{R}_n)$) and oscillator strengths $f_{1K}(\mathbf{R}_n)$ can be calculated for each point in the ensemble by calling a third-party program. Finally, the ensemble output containing geometries, momenta, energies, and oscillator strengths can be used as initial conditions for dynamics, spectrum simulations, or both.

with MQC-PE in ref 27. It is well known that after an instantaneous excitation, the cis-retinal may isomerize into trans following an exponential distribution within a 200 fs time constant and a 0.65 quantum yield as it does in bovine rhodopsin.[67] Nevertheless, MQC-PE shows that it takes 42 μs of continuous solar irradiation to populate the excited states of a single retinal molecule, which is dramatically distinct from the instantaneous excitation picture. In the vision mechanism, this slow excitation is compensated by the large number of retinal molecules in the cone cells.

4. NUCLEAR ENSEMBLES

Newton-X uses nuclear ensembles for two primary purposes, initial conditions generation for dynamics and spectrum simulations. Both are controlled by the Initcond program package. A flowchart of the processes for generating nuclear ensembles is given in Figure 5.

4.1. Initial Conditions for Dynamics. To start an FSSH trajectory, we need to provide the following:

(1) initial nuclear geometry;
(2) initial nuclear velocities;
(3) initial electronic state L;
(4) initial $\mathbf{c}$ vector [for eq 5].

The initial geometry and velocity selection are discussed in Section 4.2, as this procedure has a few variants. The initial state (L) selection is discussed in Section 4.3. By default, the initial $\mathbf{c}$ vector has $\mathrm{Re}(c_L(0)) = 1$ and null values for all other real and imaginary components. Any other value can be given as long as $\sum_K |c_K(0)|^2 = 1$. Section 4.4 reviews how geometry sampling can be used for spectrum simulations.

4.2. Sampling Nuclear Ensembles. Newton-X contains several algorithms to create initial geometries and velocities. They can be randomly generated according to some probability distribution function (PDF) or picked from a previous set of dynamics simulations.[68] The difference between them is discussed in ref 69. In certain situations, hybrid sampling using trajectories and PDFs may be required.[70] Finally, random velocities corresponding to a predetermined kinetic energy value can be generated for a fixed geometry (the algorithm is described in the appendix of ref 71).

When the molecule is initially stationary at the minimum of some state, a convenient option to generate initial geometries and velocities is to employ a Wigner PDF, assuming that the potential energy surface is harmonic around the minimum.[72,73] In this case, the Wigner probability distribution for the thermal population of the vibrational states of a molecule with N_{at} atoms and $N_F = 3N_{at} - 6$ degrees of freedom is[74,75]

$$P_W(\mathbf{Q}, \mathbf{P}) = \prod_{i=1}^{N_F} \frac{\alpha_i}{\pi\hbar} \exp\left(-\frac{\alpha_i}{\hbar\omega_i}(\omega_i^2 Q_i^2 + P_i^2)\right) \tag{20}$$

where

$$\alpha_i = \tanh\left(\frac{\hbar\omega_i}{2k_B T}\right) \tag{21}$$

In these equations, $Q_i = \mu_i^{1/2}\tilde{q}_i$ and $P_i = \mu_i^{-1/2}\tilde{p}_i$ are the mass-scaled coordinate and momentum for each normal mode i with coordinate $\tilde{q}_i$ and momentum $\tilde{p}_i$, reduced mass μ_i, and angular frequency ω_i. T is the environment temperature and k_B is the Boltzmann constant. Note that $\alpha_i = 1$ at $T = 0$. After the sampling, the normal-mode coordinates and momenta are converted to Cartesian coordinates and momenta.

The mean total energy of the sampling with eq 20 is

https://doi.org/10.1021/acs.jctc.2c00804
J. Chem. Theory Comput. 2022, 18, 6851−6865

$$\langle E\rangle = \sum_{i=1}^{N_F} \frac{\hbar\omega_i}{2\alpha_i} = \sum_i \hbar\omega_i \left(\frac{1}{2} + \frac{1}{e^{\hbar\omega_i/k_B T} - 1}\right) \tag{22}$$

which is simply the ZPE when $T = 0$. However, because $\mathbf{Q}$ and $\mathbf{P}$ are independently sampled, the total energy of the ensemble has a broad distribution of values[76] with a standard deviation

$$\sigma = \left[\sum_{i=1}^{N_F} \left(\frac{\hbar\omega_i}{2\alpha_i}\right)^2\right]^{1/2} \tag{23}$$

If a sharp distribution of total energies is required,[76] it is possible to sample the coordinates with the marginal distribution

$$P_C(\mathbf{Q}) = \int d\mathbf{P} P_W(\mathbf{Q}, \mathbf{P}) = \prod_{i=1}^{N_F} \sqrt{\frac{\alpha_i\omega_i}{\pi\hbar}}\ \exp\left(-\frac{\alpha_i\omega_i Q_i^2}{\hbar}\right) \tag{24}$$

and choose the momentum of each mode to satisfy

$$P_i = r\sqrt{\frac{\hbar\omega_i}{\alpha_i} - \omega_i^2 Q_i^2} \tag{25}$$

where r is either +1 or −1, chosen at random. All points sampled with this procedure have the same harmonic oscillator energy $\langle E\rangle$ given by eq 22. Nevertheless, when the potential energy of the sampled geometry is determined with the quantum-chemical method, anharmonic effects are introduced, and the energy distribution broadens again. To ensure a sharp distribution around $\langle E\rangle$, all Cartesian velocities can be rescaled as

$$\mathbf{v}_n^{(\text{scaled})} = \sqrt{\frac{\langle E\rangle - E_{J,n}}{K_n}}\,\mathbf{v}_n \tag{26}$$

where K_n and $E_{J,n}$ are the kinetic and quantum-chemical potential energies computed at the geometry and momentum of the sampled point n. J is the electronic state that is being sampled, usually the ground state ($J = 1$).

Newton-X also allows sampling of initial conditions for specific excited vibrational states. In this case, it is done by taking the phase-space PDF

$$P_{QHO}(\mathbf{Q}, \mathbf{P}, \mathbf{n}) = |\psi_{\mathbf{n}}(\mathbf{Q})|^2 |\xi_{\mathbf{n}}(\mathbf{P})|^2 \tag{27}$$

where $\mathbf{n}$ is a vector with the number of quanta in each normal mode and $\psi_{\mathbf{n}}(\mathbf{Q})$ and $\xi_{\mathbf{n}}(\mathbf{P})$ are the harmonic oscillator wave functions in the coordinate and momentum spaces. For $\mathbf{n} = \mathbf{0}$, the P_{QHO} distribution coincides with the Wigner PDF for the ground vibrational state.

The wave functions in eq 27 are given as the product of a Gaussian and a Hermite polynomial. One can also sample coordinates and momenta according to a Hermite function whose Gaussian exponent and center are provided by the user.[77] This feature is helpful for accelerating the convergence of certain observables as a function of the number of trajectories[78] and transforming the results from a given PDF to any desired PDF,[77] in both cases, using the importance-sampling technique.

For 1D models, a convenient way to sample initial conditions is using a Wigner distribution for a Gaussian wave packet (GWP). In this case[79]

$$P_{GWP}(x, p) = \frac{1}{\pi\hbar} e^{-(x-x_0)^2/2\Delta x^2} e^{-(p-p_0)^2/2\Delta p^2} \tag{28}$$

where x_0 and p_0 are the position and momentum GWP centers, respectively, Δx is the spatial width, and $\Delta p = \hbar/(2\Delta x)$ is the momentum width. Hence, the initial conditions are sampled from eq 28 by the rejection sampling method, drawing independent random points for both the coordinate and momentum spaces.

4.3. Choosing the Initial States. In a typical surface hopping simulation, the initial nuclear coordinates and velocities are sampled in the ground state (state 1), and the trajectory propagation starts in the excited state L. Thus, after creating the initial geometries and momenta with one of the techniques discussed in Section 4.2, we must decide on which state each trajectory will start. The most straightforward procedure is to assign a specific initial state. Nevertheless, such an approach does not consider that the character of the adiabatic state can be different in the different geometries. For instance, S_2 may be the bright state at the ground-state minimum (see Figure 6). However, S_2 may be dark in many geometries of the initial ensemble.

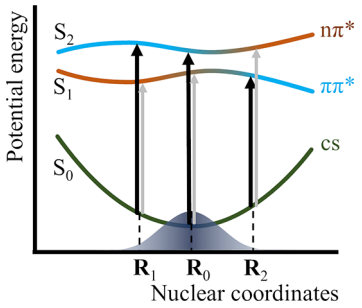

Figure 6. Selection of initial conditions in multiple states. The figure schematically shows excitations of S_0 into S_1 and S_2 for the ground-state minimum ($\mathbf{R}_0$) and two randomly sampled geometries $\mathbf{R}_1$ and $\mathbf{R}_2$. States S_1 and S_2 have regions of $\pi\pi^*$ character (cyan) where the oscillator strength is large and $n\pi^*$ character (brown), with feeble oscillator strength. To decide the initial state for a set of initial geometries (blue Gaussian distribution), Newton-X checks each geometry's excitation energies and oscillator strengths in each excited state. The algorithm picks initial states falling within a predefined excitation energy window and favors those transitions with large excitation probabilities (black arrows over the gray ones). The excitation probabilities are assumed to be proportional to the oscillator strength, and a stochastic selection is applied. The scheme is 1D, but actual cases are worked out on multidimensional potential energy surfaces.

Newton-X selects the initial state L based on the following algorithm to avoid this problem. First, it searches for excited states within an excitation energy window $\varepsilon \pm \delta\varepsilon$ above the ground state. Multiple states may appear in this excitation window for each initial geometry but with different excitation probabilities. For each initial geometry $\mathbf{R}_i$, all adiabatic states up to N_{fs} are checked. A trajectory should start in state L if the two following conditions are satisfied

$$|\Delta E_{1L}(\mathbf{R}_i) - \varepsilon| \le \delta\varepsilon \tag{29}$$

and

$$r \le \frac{f_{1L}(\mathbf{R}_i)}{f^{\max}} \tag{30}$$

https://doi.org/10.1021/acs.jctc.2c00804
J. Chem. Theory Comput. 2022, 18, 6851−6865

In these inequalities, ΔE_{1L} and f_{1L} are the excitation energy and oscillator strengths between the ground (1) and L states. R is a random number sampled from a uniform distribution in the [0,1] interval. $f^{\max}$ is the maximum oscillator strength value among all sampled geometries and states. The first inequality ensures that the initial state is in the excitation window of interest. The second inequality selects preferentially states with large transition probabilities (proportional to the oscillator strength[80]). This algorithm leads to an ensemble of trajectories starting in several adiabatic states (Figure 6). In principle, the sampling may take the same geometry and velocity as the initial condition for multiple states. This redundancy does not cause any conflict because the initial conditions for each state are written in separate lists.

Alternatively, the initial state can be selected from a probability distribution given by a black body radiance at temperature T.[27] In this case, inequality (30) is replaced with

$$r \leq \frac{f_{1L}(\mathbf{R}_i)\Delta E_{1L}(\mathbf{R}_i)^2(e^{\Delta E_{1L}(\mathbf{R}_i)/k_B T}-1)^{-1}}{[f\Delta E^2(e^{\Delta E/k_B T}-1)^{-1}]^{\max}} \tag{31}$$

The denominator in this expression is the maximum value that $f_{1K}\Delta E_{1K}^2(e^{\Delta E_{1K}/k_B T}-1)^{-1}$ can reach among all geometries and states in the ensemble.

4.4. Spectrum Simulation. The same ensembles sampled for choosing the initial conditions can also be used to simulate spectra within the NEA.[72] NEA comprises an incoherent sum of transition probabilities for each geometry in the ensemble from a source state into one or more target states. NEA allows obtaining the spectral band envelopes in a post-Condon approximation but without vibrational resolution.

For steady-state photoabsorption spectrum simulations, the NEA absorption cross section is[72]

$$\sigma^{\mathrm{pa}}(E) = \frac{\pi e^2 \hbar}{2m_e c\varepsilon_0 E}\sum_K^{N_{\mathrm{fs}}}\frac{1}{N_{\mathrm{p}}^{(K)}}\sum_n^{N_{\mathrm{p}}^{(K)}}\Delta E_{1K}(\mathbf{R}_n) f_{1K}(\mathbf{R}_n)\, w_s(E-\Delta E_{1K}(\mathbf{R}_n),\delta) \tag{32}$$

where E is the photon energy, ε_0 is the vacuum permittivity, c is the speed of light, and e and m_e are the electron charge and mass, respectively. w_s is a normalized sharp line shape (a Lorentzian function, for instance) centered at the vertical transition energy ΔE_{1K} between the ground state (state 1) and the electronic state K, computed for each of the ensemble geometries $\mathbf{R}_n$. f_{1K} is the oscillator strength between the two states at the same geometry. A total of N_{fs} electronic states are included. The ensemble contains $N_{\mathrm{p}}^{(K)}$ geometries for state K. The parameter δ is the width of the line shape function w_s.

For steady-state emission, the NEA differential emission rate into the ground state is[72]

$$\Gamma_{\mathrm{rad}}(E) = \frac{e^2}{2\pi\hbar m_e c^3\varepsilon_0}[1-H(E-h\nu_a)]\frac{1}{N_T}\sum_K^{N_{\mathrm{fs}}}\sum_n^{N_{\mathrm{p}}^{(K)}}\Delta E_{K1}(\mathbf{R}_n)^2|f_{K1}(\mathbf{R}_n)|\, w_s(E-\Delta E_{K1}(\mathbf{R}_n),\delta) \tag{33}$$

where $H(E-h\nu_a)$ is the Heaviside step function ensuring that the emission energy is smaller than the excitation energy $h\nu_a$. N_T is the total number of geometries in the ensemble, that is

$$N_T = \sum_K^{N_{\mathrm{fs}}} N_{\mathrm{p}}^{(K)} \tag{34}$$

Within this formulation, the area under the emission spectrum reflects the emission lifetime. The emission rate is given by

$$\kappa_{\mathrm{rad}} = \frac{1}{\hbar}\int \Gamma_{\mathrm{rad}}(E)\, dE \tag{35}$$

Note that the sum over the states K in eq 33 implies that non-Kasha emissions[81] are also considered. See ref 49 for an example of simulations including fluorescence from the first and second excited states of pyrene.

Phosphorescence spectrum can also be obtained with eq 33. In this case, the spin-forbidden oscillator strength between T_1 and S_0 is computed within the first-order perturbation theory [see eq 65 of ref 82].

The effect of medium on spectral intensities can be accounted for via the refractive index n_r. For absorption [eq 32], the intensities are multiplied by n_r^{-1}. For emission [eq 33], they are multiplied by n_r^3. Alternatively, more involved approaches can be used by post-processing the results with better local field corrections.[83]

Reference 84 discusses the NEA implementation of steady-state and time-dependent photoionization spectrum simulations in Newton-X. The ionization probability is determined either from the Dyson orbitals' norm (computed by Newton-X) or photoionization cross sections.

5. ELECTRONIC STRUCTURE AND INTERFACES

Newton-X CS can simulate surface hopping dynamics and spectra using model potentials and diverse electronic structure methods, as listed in Table 1. The choice of each one depends on the specific problem, always requiring a trade-off between

Table 1. Programs and Methods Interfaced to Newton-X CS[a]

program	methods	couplings
COLUMBUS[b95]	MRCI, MCSCF + MM	third-party **h**, overlap (DD), TD-BA
BAGEL[b96]	XMS-CASPT2	third-party **h**,TD-BA
GAMESS[b97]	MCSCF	third-party **h**,TD-BA
TURBOMOLE[98]	ADC(2) + MM	overlap (DD, OD), TD-BA
	TDDFT, TDA + MM	overlap (DD, OD), TD-BA
GAUSSIAN[99]	(U)TDDFT, (U)TDA, (U)CIS	overlap (DD, OD), TD-BA
	TDDFT + PFF[d]	overlap (DD, OD), TD-BA
	MCSCF	third-party **h**,TD-BA
MOPAC (Pisa)[c]	FOMO-CI, EXASH	third-party **h**,third-party overlap, TD-BA
MNDO[d89]	OM*x*/MRCI	third-party **h**,TD-BA
DFTB+[b100]	TD-DFTB	overlap (DD, OD), TD-BA
MLatom[b101]	ML	third-party **h**,TD-BA
built-in codes[b]	collection of analytical models	third-party **h**,TD-BA

[a]For each third-party program, the table gives the methods allowing surface hopping dynamics and the types of coupling employed by Newton-X CS. When wave function overlaps are available, FSSH can be based either on time derivative couplings or LD. [b]These programs are free and open source. [c]Development version. [d]Only in Newton-X NS. MM—molecular mechanics with Tinker.[102] (U)—indicates optional unrestricted. PFF—polarizable force field with AMOEBA.

https://doi.org/10.1021/acs.jctc.2c00804
J. Chem. Theory Comput. 2022, 18, 6851−6865

quality and computational costs. The third-party programs are not distributed with Newton-X.

The multireference methods[85] (ab initio MRCI,[86] MCSCF, CASPT2,[87] and semiempirical FOMO-CI[88] and OM*x*/MRCI[89]) describe the entire internal conversion process until the system returns to the ground state. The single-reference methods [ADC(2),[90] TDDFT,[91] TD-DFTB,[92] TDA, and CIS] describe the internal conversion between excited states but not the transition to the ground state.[91]

Thus, Newton-X can be used for a wide variety of simulations (Figure 7). On the one hand, it can simulate the short timescale dynamics of a small photoexcited molecule but with a high-level method such as the complete active space perturbation theory to the second order (CASPT2). On the other hand, Newton-X can simulate the dynamics of a large molecule for longer times but using a low-level electronic structure method such as the time-dependent density functional tight binding (TD-DFTB).

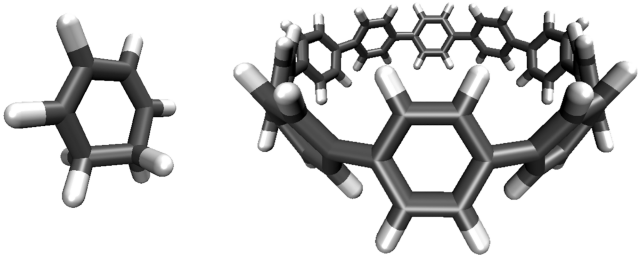

Figure 7. Newton-X operation range. Newton-X CS can simulate the nonadiabatic dynamics of a small system such as cyclohexadiene (left) with a high-level method such as CASPT2 (14 atoms, 3 electronic states, 150 trajectories, 0.4 ps/trajectory, and 0.5 fs time step).[93] It can also simulate the nonadiabatic dynamics of a large molecule, cycloparaphenylene, for example (right), with a low-level method such as TD-DFTB (100 atoms, 7 electronic states, 50 trajectories, 3 ps/trajectory, and 0.5 fs time step).[94]

Dynamics can also be carried out with several analytical models available in Newton-X, including the 1D models by Tully,[34] the 1D double arch,[45] the 1D Nikitin Hamiltonian,[103] the 2D conical intersection,[36] the *N*-dimensional Spin−Boson Hamiltonian,[104] and several complex-valued 1D models for CS-FSSH.[28]

DFT/MRCI[105,106] can be used for spectrum simulations but not for dynamics due to the lack of analytical energy gradients in that method. Phosphorescence spectra can be simulated using Newton-X interfaced to PySOC to obtain spin−orbit couplings[60] and PySOC calling Gaussian for TDDFT calculations.[99] Photoionization cross sections from EzDyson[107] can be used to simulate the photoionization spectra.

Electronic properties during dynamics can be analyzed with TheoDORE (theodore-qc.sourceforge.net),[108] which uses one-particle transition density matrices[109] to deliver many electronic state descriptors for exciton characterization. For computational efficiency, TheoDORE's analysis is not performed simultaneously with the dynamics simulations, but it is done afterward on subsets of geometries sampled from the trajectories.

5.1. Hybrid Approaches for Surface Hopping. Surface hopping dynamics can be propagated in Newton-X CS using energy gradients from hybrid quantum mechanics (QM) and molecular mechanics (MM) combinations (see Table 1).[70] The most common hybrid QM/MM approach is the electrostatic embedding,[110] in which the charges of the MM region are included in the QM Hamiltonian.

Alternatively, Newton-X NS allows employing AMOEBA[111] force field to simulate environmental effects using a fully polarizable electrostatic description. In this scheme, each atomic site of the environment is represented using a set of fixed electrostatic multipoles (up to quadrupoles) and isotropic polarizability. As a response to the electric field generated by the QM density (and the fixed multipoles of the environment), the presence of isotropic polarizabilities leads to a set of induced point dipoles that, in turn, affect the QM density. This mutual polarization between the QM density and the environment enhances the completeness of the environment's response with respect to an electrostatic-only model. It is expected to be particularly important in the description of light-induced processes.[112] At present, TDDFT simulations can be coupled with the AMOEBA force field, using a previously developed interface between Tinker and Gaussian.[113]

The current implementation of surface hopping with TD-DFT/AMOEBA has been tested using the example of the water photo-oxidation of pyrimidine.[114] Even if the method is still at the beginning of its development, we expect to provide a valuable framework for studying the photochemical processes of molecular systems in solution or embedded in more complex biological or artificial matrices.

5.2. Exciton Approach for Surface Hopping. The exciton approach for surface hopping (EXASH)[29] is a fragment-based method, where electronic properties at each time step are derived, permuting each chromophore in the field of the others. It is set to work with semiempirical FOMO-CI and MM fields to describe systems composed of many chromophores using an excitonic approach. In Newton-X NS, EXASH is also implemented for TDDFT/MM.

In principle, the number of chromophores considered in EXASH is limited only by the computational resources: if another chromophore is added to the system, one has mainly to add the related QM/MM calculation (at each integration time step). The price is that only states that can be written as linear combinations of local excitations can be considered. The first application of EXASH[29] consisted of the simulation of the dynamics of an azobenzene dimer held together by sulfur bridges. EXASH revealed that although fast, the excitation transfer between chromophores is limited to the $\pi\pi^*$ manifold and absent for $n\pi^*$ states.

6. MACHINE LEARNING

6.1. Spectrum with Supervised ML. An interface between Newton-X and the MLatom[101] (mlatom.com) allows simulating NEA spectra (see Section 4.4) driven by supervised ML predictions.[115] The ML-NEA method uses transition energies and oscillator strengths computed with electronic structure methods for a minimum ensemble (typically, several hundreds of geometries) to train ML models to predict transition energies and oscillator strengths for the NEA spectrum simulation with statistically convergent ensembles (50k geometries or more) at minimum additional cost. The ML-NEA algorithm automatically determines the size of the minimum ensemble. The ML-NEA results are independent of the arbitrary line-width parameter δ [eq 32]. A tutorial for applying ML-NEA is available on the MLatom website.

6.2. Dynamics with Supervised ML. Nonadiabatic dynamics simulations based on ML potentials are still in

https://doi.org/10.1021/acs.jctc.2c00804
J. Chem. Theory Comput. 2022, 18, 6851−6865

their early development stage.[116,117] As developers, our goal has been to create a flexible software interface, paving the way for easily plugin new models into an automated framework to accelerate the performance tests and deploy ML potentials. The interface between Newton-X CS and MLatom enables ML for nonadiabatic dynamics bearing these goals in mind. Potential energies, energy gradients, and state couplings can be obtained with diverse kernel methods and neural networks, with various local and global descriptors.[118] In this interface, Newton-X does not know that the electronic properties are ML-based. It calls MLatom as if it were a conventional electronic structure program.

ML-based nonadiabatic dynamics is still not a routine task due to the intrinsic difficulties of accurately predicting multiple excited states.[117] At the moment of writing, there are no unique protocols to create training sets, and this task requires intense legwork for each new molecular system. Moreover, transferability between systems is still challenging, although recent investigations have demonstrated encouraging proof-of-concept results.[119] Nevertheless, once the ML model is ready, it allows semiquantitatively predicting the nonadiabatic dynamics at much lower computational costs than with a quantum-chemical method.[120]

Training and predicting nonadiabatic coupling vectors demand special attention because of their narrowly peaked functional features and arbitrary phases.[116] Alternatively, Newton-X allows computing couplings with TD-BA,[25] which, as discussed in Section 3.6, only depends on the excitation energies and their time derivatives.

6.3. Data Analysis and Unsupervised ML. Newton-X has native programs to perform basic statistical analysis of the simulated trajectories. They deliver averages and standard deviations over trajectories for energies, populations, and geometric parameters as a function of time.

These statistical programs are left in Newton-X CS as a legacy feature. They have been replaced by Ulamdyn (www.ulamdyn.com), an independent analysis open-source program also developed by the Newton-X team. Ulamdyn is not only more efficient than the native statistical codes but it has several additional functionalities. In particular, it extends the analysis to a broader set of statistical descriptors, delivering information about the data distribution's central tendency, skewness, and sharpness, as well as the accuracy measure of the estimated mean via bootstrap simulation (see an example in Figure 4).

As a major feature, Ulamdyn provides a complete integrated pipeline starting from the data curation to perform advanced unsupervised learning analysis of the molecular dynamics data. Several dimensionality-reduction and data-clustering algorithms were implemented for this task based on the popular Python package Scikit-Learn (scikit-learn.org). These analyses have proven extremely useful for unraveling hidden patterns in nonadiabatic dynamics data in a very efficient and automated manner.[121−123] All the details about the Ulamdyn features and implementations will be discussed in a separate publication.

7. NEWTON-X FUTURE

Newton-X was initially developed in a context where the electronic structure calculations were much more computationally expensive than integrating the EOM. For this reason, the Newton-X architecture has privileged modularity over efficiency. Thus, a new interface could be quickly built at the price of intensive disk reading and writing. In the end, the time spent on quantum chemical calculations more than compensated for this computational overhead.

This situation changed with the development of extremely fast parameterized quantum chemical methods (such as TD-DFTB) and the advent of ML potentials. Now, computational overheads may have a significant impact on the costs. To tackle this issue, we are developing Newton-X NS, which aims at extreme computational efficiency and better data management standards. Newton-X NS will be presented in a separate paper in the future, but we will highlight some features here.

The development of Newton-X NS aims at efficency . More precisely, we bear three goals in mind: (1) maximize computational performance (optimizing, in particular, the input/output operations), (2) deliver data management standards that allow for easier sharing and more streamlined data production, and (3) keep the entry barrier for new developers as low as possible. The first goal leads us to switch from a collection of Perl scripts to a monolithic Fortran code, allowing direct data exchange between the different parts of the code through memory, not text files. This redesign effectively reduces the time spent in read/write operations, which is particularly useful when using built-in analytical models. In those cases, no external electronic structure code is invoked, and the dynamics can be up to 2000 times faster than with Newton-X CS.[124]

Having a monolithic code also helps with the second goal. We chose the H5MD file format[125] based on the Hierarchical Data Format 5 (HDF5) framework. Our monolithic implementation allows us to open the interface only once, and we can write the outcome of the dynamics to disk at one specific point in the code. In that way, we can be sure that the data written is always consistent. This data format is widely supported and implemented in several quantum-chemistry software (such as LAMMPS,[126] Molcas,[127] and MLatom[101]), so we can benefit from the tools already developed for tasks such as visualization of the dynamics (VMD[128] plugin). The HDF5 library also binds to popular scripting languages such as Python or Julia.

To keep the low entry barrier to code development, we offer a clear and up-to-date developer documentation using automatic tools [FORD (github.com/Fortran-FOSS-Programmers/ford), for instance] to generate the documentation directly from the comments inside the code. We follow guidelines inspired by object-oriented programming practice, where each step of the computation is performed in its own module with a clearly defined entry point. Finally, all parameters used in the dynamics, as well as the default values and descriptions, are defined in a collection of easy-to-read YAML files, which a Perl driver parses to generate a proper input file for the Fortran program based on the user's defined parameters. This input management helps to keep inputs consistent from version to version, as changes are transparent to the end user.

The development of Newton-X NS is hosted on Gitlab (gitlab.com/light-and-molecules/newtonx) and will be released soon under GPL3. The features of the Newton-X CS will be gradually transferred to NS. Nevertheless, the two series should coexist until this algorithmic transfer is fully accomplished.

https://doi.org/10.1021/acs.jctc.2c00804
J. Chem. Theory Comput. 2022, 18, 6851−6865

AUTHOR INFORMATION

Corresponding Author

Mario Barbatti − *Aix Marseille University, CNRS, ICR, 13013 Marseille, France; Institut Universitaire de France, 75231 Paris, France;* orcid.org/0000-0001-9336-6607; Email: mario.barbatti@univ-amu.fr; https://www.barbatti.org

Authors

Mattia Bondanza − *Dipartimento di Chimica e Chimica Industriale, Università di Pisa, 56124 Pisa, Italy*

Rachel Crespo-Otero − *Department of Chemistry, Queen Mary University of London, E1 4NS London, U.K.;* orcid.org/0000-0002-8725-5350

Baptiste Demoulin − *Aix Marseille University, CNRS, ICR, 13013 Marseille, France*

Pavlo O. Dral − *State Key Laboratory of Physical Chemistry of Solid Surfaces, Fujian Provincial Key Laboratory of Theoretical and Computational Chemistry, Department of Chemistry, and College of Chemistry and Chemical Engineering, Xiamen University, 361005 Xiamen, China;* orcid.org/0000-0002-2975-9876

Giovanni Granucci − *Dipartimento di Chimica e Chimica Industriale, Università di Pisa, 56124 Pisa, Italy;* orcid.org/0000-0002-4753-6318

Fábris Kossoski − *Laboratoire de Chimie et Physique Quantiques (UMR 5626), Université de Toulouse, CNRS, UPS, 31000 Toulouse, France;* orcid.org/0000-0002-1627-7093

Hans Lischka − *Department of Chemistry and Biochemistry, Texas Tech University, Lubbock, Texas 79409, United States;* orcid.org/0000-0002-5656-3975

Benedetta Mennucci − *Dipartimento di Chimica e Chimica Industriale, Università di Pisa, 56124 Pisa, Italy;* orcid.org/0000-0002-4394-0129

Saikat Mukherjee − *Aix Marseille University, CNRS, ICR, 13013 Marseille, France;* orcid.org/0000-0002-0025-4735

Marek Pederzoli − *J. Heyrovsky Institute of Physical Chemistry, Academy of Sciences of the Czech Republic, 18223 Prague 8, Czech Republic*

Maurizio Persico − *Dipartimento di Chimica e Chimica Industriale, Università di Pisa, 56124 Pisa, Italy;* orcid.org/0000-0001-6861-9289

Max Pinheiro Jr − *Aix Marseille University, CNRS, ICR, 13013 Marseille, France*

Jiří Pittner − *J. Heyrovsky Institute of Physical Chemistry, Academy of Sciences of the Czech Republic, 18223 Prague 8, Czech Republic*

Felix Plasser − *Department of Chemistry, Loughborough University, LE11 3TU Loughborough, U.K.;* orcid.org/0000-0003-0751-148X

Eduarda Sangiogo Gil − *Dipartimento di Chimica e Chimica Industriale, Università di Pisa, 56124 Pisa, Italy*

Ljiljana Stojanovic − *Department of Physics and Astronomy, University College London, WC1E 6BT London, U.K.;* orcid.org/0000-0003-2821-5110

Complete contact information is available at: https://pubs.acs.org/10.1021/acs.jctc.2c00804

Funding

M.B., B.D., S.M., and M.P. are financially supported by the European Research Council under grant agreement no. 832237 (SubNano). They also acknowledge the Centre de Calcul Intensif d'Aix-Marseille for granting access to its high-performance computing resources. M.B. acknowledges the support from the Excellence Initiative of Aix-Marseille University (A*MIDEX) funded by the French Government's "Investissements d'Avenir" program. M.B. and F.K. acknowledge funding from the Agence Nationale de la Recherche (ANR) under the WSPLIT project (ANR-17-CE05-0005-01). Mattia Bondanza and Benedetta Mennucci acknowledge funding by the European Research Council under grant ERC-AdG-786714 (LIFETimeS). R.C.-O. was supported by Leverhulme Trust (RPG-2019-122) and EPSRC (EP/R029385/1). P.O.D. acknowledges funding from the National Natural Science Foundation of China (no. 22003051), the Fundamental Research Funds for the Central Universities (no. 20720210092), and via the Lab project of the State Key Laboratory of Physical Chemistry of Solid Surfaces. G.G. acknowledges funding from the University of Pisa (PRA_2020_21). J.P. and M.P. acknowledge the support from the Czech Science Foundation, grant no. 19-06860S.

Notes

The authors declare no competing financial interest.

Newton-X CS (including Initcond) can be downloaded free of charge at www.newtonx.org. Ulamdyn is available at www.ulamdyn.com.

ACRONYMS

ADC(2), algebraic diagrammatic constructions to second order; CASPT2, complete active space perturbation theory to second order; CI, configuration interaction; CIS, CI with single excitations; CS, classical series; CS-FSSH, complex-valued surfaces FSSH; DC, decoherence corrected; DD, determinant derivative; DFT/MRCI, combined density functional theory and multireference CI; EOM, equations of motion; EXASH, exciton approach for surface hopping; FOMO-CI, floating occupation CI; FSSH, fewest switches surface hopping; GPL3, GNU general public license 3; GWP, Gaussian wave packet; HDF5, hierarchical data format 5; LD, local diabatization; LP-ZPE, local-pair ZPE; MCSCF, multiconfigurational self-consistent field; ML, machine learning; MM, molecular mechanics; MQC-PE, mixed quantum-classical pulsed ensemble; MRCI, multireference CI; NEA, nuclear ensemble approach; NS, new series; OD, orbital derivative; ODC, overlap-driven decoherence correction; OMx, orthogonalization method x; PDF, probability distribution function; PFF, polarizable force field; QM/MM, quantum mechanics/molecular mechanics; SDM, simplified decay of mixing; TDA, Tamm−Dancoff approximation; TD-BA, time-dependent Baeck-An; TDDFT, time-dependent density functional theory; TD-DFTB, time-dependent density functional tight-binding; TSH, trajectory surface hopping; YAML, YAML ain't markup language; ZPE, zero-point energy

REFERENCES

(1) Crespo-Otero, R.; Barbatti, M. Recent Advances and Perspectives on Nonadiabatic Mixed Quantum-Classical Dynamics. *Chem. Rev.* **2018**, *118*, 7026−7068.

(2) Nelson, T. R.; White, A. J.; Bjorgaard, J. A.; Sifain, A. E.; Zhang, Y.; Nebgen, B.; Fernandez-Alberti, S.; Mozyrsky, D.; Roitberg, A. E.; Tretiak, S. Non-adiabatic Excited-State Molecular Dynamics: Theory and Applications for Modeling Photophysics in Extended Molecular Materials. *Chem. Rev.* **2020**, *120*, 2215−2287.

(3) Wang, L.; Akimov, A.; Prezhdo, O. V. Recent Progress in Surface Hopping: 2011−2015. *J. Phys. Chem. Lett.* **2016**, *7*, 2100−2112.
(4) Granucci, G.; Persico, M.; Toniolo, A. Direct Semiclassical Simulation of Photochemical Processes with Semiempirical Wave Functions. *J. Chem. Phys.* **2001**, *114*, 10608−10615.
(5) Barbatti, M.; Granucci, G.; Persico, M.; Ruckenbauer, M.; Vazdar, M.; Eckert-Maksić, M.; Lischka, H. The on-the-Fly Surface-Hopping Program System Newton-X: Application to Ab Initio Simulation of the Nonadiabatic Photodynamics of Benchmark Systems. *J. Photochem. Photobiol., A* **2007**, *190*, 228−240.
(6) Barbatti, M.; Ruckenbauer, M.; Plasser, F.; Pittner, J.; Granucci, G.; Persico, M.; Lischka, H. Newton-X: a surface-hopping program for nonadiabatic molecular dynamics. *Wiley Interdiscip. Rev. Comput. Mol. Sci.* **2014**, *4*, 26−33.
(7) Zheng, J.; Li, Z.-H.; Jasper, A. W.; Bonhommeau, D. A.; Valero, R.; Meana-Pañeda, R.; Mielke, S. L.; Zhang, L.; Truhlar, D. G.*ANT*, Version 2019; University of Minnesota: Minneapolis, 2019. http://comp.chem.umn.edu/ant.
(8) Doltsinis, N. L.; Marx, D. Nonadiabatic Car-Parrinello Molecular Dynamics. *Phys. Rev. Lett.* **2002**, *88*, 166402.
(9) Gardner, J.; Douglas-Gallardo, O. A.; Stark, W. G.; Westermayr, J.; Janke, S. M.; Habershon, S.; Maurer, R. NQCDynamics.jl: A Julia package for nonadiabatic quantum classical molecular dynamics in the condensed phase. *J. Chem. Phys.* **2022**, *156*, 174801.
(10) Lee, I. S.; Ha, J.-K.; Han, D.; Kim, T. I.; Moon, S. W.; Min, S. K. PyUNIxMD A Python-based excited state molecular dynamics package. *J. Comput. Chem.* **2021**, *42*, 1755−1766.
(11) Malone, W.; Nebgen, B.; White, A.; Zhang, Y.; Song, H.; Bjorgaard, J. A.; Sifain, A. E.; Rodriguez-Hernandez, B.; Freixas, V. M.; Fernandez-Alberti, S.; Roitberg, A. E.; Nelson, T. R.; Tretiak, S. NEXMD Software Package for Non-adiabatic Excited State Molecular Dynamics Simulations. *J. Chem. Theory Comput.* **2020**, *16*, 5771−5783.
(12) Menger, M. F. S. J.; Ehrmaier, J.; Faraji, S. PySurf: A Framework for Database Accelerated Direct Dynamics. *J. Chem. Theory Comput.* **2020**, *16*, 7681−7689.
(13) Weingart, O.; Nenov, A.; Altoè, P.; Rivalta, I.; Segarra-Martí, J.; Dokukina, I.; Garavelli, M. COBRAMM 2.0 — A software interface for tailoring molecular electronic structure calculations and running nanoscale (QM/MM) simulations. *J. Mol. Model.* **2018**, *24*, 271.
(14) Humeniuk, A.; Mitrić, R. DFTBaby: A Software Package for Non-adiabatic Molecular Dynamics Simulations Based on Long-Range Corrected Tight-binding TD-DFT(B). *Comput. Phys. Commun.* **2017**, *221*, 174−202.
(15) Akimov, A. V. Libra: An Open-Source "Methodology Discovery" Library for Quantum and Classical Dynamics Simulations. *J. Comput. Chem.* **2016**, *37*, 1626−1649.
(16) Du, L.; Lan, Z. An On-the-Fly Surface-Hopping Program JADE for Nonadiabatic Molecular Dynamics of Polyatomic Systems: Implementation and Applications. *J. Chem. Theory Comput.* **2015**, *11*, 1360−1374.
(17) Akimov, A. V.; Prezhdo, O. V. Advanced Capabilities of the PYXAID Program: Integration Schemes, Decoherence Effects, Multiexcitonic States, and Field-Matter Interaction. *J. Chem. Theory Comput.* **2014**, *10*, 789−804.
(18) Richter, M.; Marquetand, P.; González-Vázquez, J.; Sola, I.; González, L. SHARC: Ab Initio Molecular Dynamics with Surface Hopping in the Adiabatic Representation Including Arbitrary Couplings. *J. Chem. Theory Comput.* **2011**, *7*, 1253−1258.
(19) Tapavicza, E.; Tavernelli, I.; Rothlisberger, U. Trajectory Surface Hopping within Linear Response Time-Dependent Density-Functional Theory. *Phys. Rev. Lett.* **2007**, *98*, 023001−023004.
(20) Fingerhut, B. P.; Dorfman, K. E.; Mukamel, S. Monitoring Nonadiabatic Dynamics of the RNA Base Uracil by UV Pump−IR Probe Spectroscopy. *J. Phys. Chem. Lett.* **2013**, *4*, 1933−1942.
(21) Fingerhut, B. P.; Oesterling, S.; Haiser, K.; Heil, K.; Glas, A.; Schreier, W. J.; Zinth, W.; Carell, T.; de Vivie-Riedle, R. ONIOM approach for non-adiabatic on-the-fly molecular dynamics demonstrated for the backbone controlled Dewar valence isomerization. *J. Chem. Phys.* **2012**, *136*, 204307.
(22) Ryabinkin, I. G.; Joubert-Doriol, L.; Izmaylov, A. F. Geometric Phase Effects in Nonadiabatic Dynamics near Conical Intersections. *Acc. Chem. Res.* **2017**, *50*, 1785−1793.
(23) Park, J. W.; Shiozaki, T. On-the-Fly CASPT2 Surface-Hopping Dynamics. *J. Chem. Theory Comput.* **2017**, *13*, 3676−3683.
(24) Nakashima, Y.; Okutsu, K.; Fujimoto, K.; Ito, Y.; Kanno, M.; Nakano, M.; Ohshimo, K.; Kono, H.; Misaizu, F. Visible photodissociation of the CO_2 dimer cation: fast and slow dissociation dynamics in the excited state. *Phys. Chem. Chem. Phys.* **2019**, *21*, 3083−3091.
(25) do Casal, M. T.; Toldo, J. M.; Pinheiro, M., Jr.; Barbatti, M. Fewest switches surface hopping with Baeck-An couplings [version 1; peer review: 3 approved]. *Open Res. Europe* **2021**, *1*, 49.
(26) Mukherjee, S.; Barbatti, M. A Hessian-Free Method to Prevent Zero-Point Energy Leakage in Classical Trajectories. *J. Chem. Theory Comput.* **2022**, *18*, 4109−4116.
(27) Barbatti, M. Simulation of Excitation by Sunlight in Mixed Quantum-Classical Dynamics. *J. Chem. Theory Comput.* **2020**, *16*, 4849−4856.
(28) Kossoski, F.; Barbatti, M. Nonadiabatic dynamics in multi-dimensional complex potential energy surfaces. *Chem. Sci.* **2020**, *11*, 9827−9835.
(29) Gil, E.; Granucci, G.; Persico, M. Surface Hopping Dynamics with the Frenkel Exciton Model in a Semiempirical Framework. *J. Chem. Theory Comput.* **2021**, *17*, 7373−7383.
(30) Verlet, L. Computer Experiments on Classical Fluids .I. Thermodynamical Properties of Lennard-Jones Molecules. *Phys. Rev.* **1967**, *159*, 98−103.
(31) Swope, W. C.; Andersen, H. C.; Berens, P. H.; Wilson, K. R. A Computer-Simulation Method for the Calculation of Equilibrium-Constants for the Formation of Physical Clusters of Molecules - Application to Small Water Clusters. *J. Chem. Phys.* **1982**, *76*, 637−649.
(32) Andersen, H. C. Molecular-Dynamics Simulations at Constant Pressure and/or Temperature. *J. Chem. Phys.* **1980**, *72*, 2384−2393.
(33) Czakó, G.; Kaledin, A. L.; Bowman, J. M. A practical method to avoid zero-point leak in molecular dynamics calculations: Application to the water dimer. *J. Chem. Phys.* **2010**, *132*, 164103.
(34) Tully, J. C. Molecular-Dynamics with Electronic-Transitions. *J. Chem. Phys.* **1990**, *93*, 1061−1071.
(35) Tully, J. C. Mixed Quantum-Classical Dynamics. *Faraday Discuss.* **1998**, *110*, 407−419.
(36) Ferretti, A.; Granucci, G.; Lami, A.; Persico, M.; Villani, G. Quantum mechanical and semiclassical dynamics at a conical intersection. *J. Chem. Phys.* **1996**, *104*, 5517−5527.
(37) Butcher, J. C. A Modified Multistep Method for the Numerical Integration of Ordinary Differential Equations. *J. ACM* **1965**, *12*, 124−135.
(38) Subotnik, J. E.; Jain, A.; Landry, B.; Petit, A.; Ouyang, W.; Bellonzi, N. Understanding the Surface Hopping View of Electronic Transitions and Decoherence. *Annu. Rev. Phys. Chem.* **2016**, *67*, 387−417.
(39) Bittner, E. R.; Rossky, P. J. Quantum decoherence in mixed quantum-classical systems: Nonadiabatic processes. *J. Chem. Phys.* **1995**, *103*, 8130−8143.
(40) Granucci, G.; Persico, M. Critical appraisal of the fewest switches algorithm for surface hopping. *J. Chem. Phys.* **2007**, *126*, 134114.
(41) Granucci, G.; Persico, M.; Zoccante, A. Including quantum decoherence in surface hopping. *J. Chem. Phys.* **2010**, *133*, 134111.
(42) Zhu, C. Y.; Nangia, S.; Jasper, A. W.; Truhlar, D. G. Coherent Switching with Decay of Mixing: An Improved Treatment of Electronic Coherence for Non-Born-Oppenheimer Trajectories. *J. Chem. Phys.* **2004**, *121*, 7658−7670.
(43) Hack, M. D.; Truhlar, D. G. A natural decay of mixing algorithm for non-Born−Oppenheimer trajectories. *J. Chem. Phys.* **2001**, *114*, 9305−9314.

https://doi.org/10.1021/acs.jctc.2c00804
J. Chem. Theory Comput. 2022, 18, 6851−6865

(44) Jasper, A. W.; Truhlar, D. G. Electronic decoherence time for non-Born-Oppenheimer trajectories. *J. Chem. Phys.* **2005**, *123*, 064103.
(45) Subotnik, J. E.; Shenvi, N. A new approach to decoherence and momentum rescaling in the surface hopping algorithm. *J. Chem. Phys.* **2011**, *134*, 024105.
(46) Barbatti, M. Velocity Adjustment in Surface Hopping: Ethylene as a Case Study of the Maximum Error Caused by Direction Choice. *J. Chem. Theory Comput.* **2021**, *17*, 3010−3018.
(47) Plasser, F.; Mai, S.; Fumanal, M.; Gindensperger, E.; Daniel, C.; González, L. Strong Influence of Decoherence Corrections and Momentum Rescaling in Surface Hopping Dynamics of Transition Metal Complexes. *J. Chem. Theory Comput.* **2019**, *15*, 5031−5045.
(48) Carof, A.; Giannini, S.; Blumberger, J. Detailed balance, internal consistency, and energy conservation in fragment orbital-based surface hopping. *J. Chem. Phys.* **2017**, *147*, 214113.
(49) Braun, G.; Borges, I., Jr.; Aquino, A.; Lischka, H.; Plasser, F.; do Monte, S. A.; Ventura, E.; Mukherjee, S.; Barbatti, M. Non-Kasha fluorescence of pyrene emerges from a dynamic equilibrium between excited states. *J. Chem. Phys.* **2022**, DOI: 10.1063/5.0113908.
(50) Plasser, F.; Granucci, G.; Pittner, J.; Barbatti, M.; Persico, M.; Lischka, H. Surface Hopping Dynamics Using a Locally Diabatic Formalism: Charge Transfer in the Ethylene Dimer Cation and Excited State Dynamics in the 2-Pyridone Dimer. *J. Chem. Phys.* **2012**, *137*, 22A514−13.
(51) Wang, L.; Prezhdo, O. V. A Simple Solution to the Trivial Crossing Problem in Surface Hopping. *J. Phys. Chem. Lett.* **2014**, *5*, 713−719.
(52) Fernandez-Alberti, S.; Roitberg, A. E.; Nelson, T.; Tretiak, S. Identification of Unavoided Crossings in Nonadiabatic Photoexcited Dynamics Involving Multiple Electronic States in Polyatomic Conjugated Molecules. *J. Chem. Phys.* **2012**, *137*, 014512.
(53) Aguilera-Porta, N.; Corral, I.; Munoz-Muriedas, J.; Granucci, G. Excited state dynamics of some nonsteroidal anti-inflammatory drugs: A surface-hopping investigation. *Comput. Theor. Chem.* **2019**, *1152*, 20−27.
(54) Hammes-Schiffer, S.; Tully, J. C. Proton-Transfer in Solution - Molecular-Dynamics with Quantum Transitions. *J. Chem. Phys.* **1994**, *101*, 4657−4667.
(55) Pittner, J.; Lischka, H.; Barbatti, M. Optimization of Mixed Quantum-Classical Dynamics: Time-Derivative Coupling Terms and Selected Couplings. *Chem. Phys.* **2009**, *356*, 147−152.
(56) Stojanović, L.; Bai, S.; Nagesh, J.; Izmaylov, A. F.; Crespo-Otero, R.; Lischka, H.; Barbatti, M. New Insights into the State Trapping of UV-Excited Thymine. *Molecules* **2016**, *21*, 1603.
(57) Ryabinkin, I. G.; Nagesh, J.; Izmaylov, A. F. Fast Numerical Evaluation of Time-Derivative Nonadiabatic Couplings for Mixed Quantum−Classical Methods. *J. Phys. Chem. Lett.* **2015**, *6*, 4200−4203.
(58) Werner, U.; Mitrić, R.; Suzuki, T.; Bonačić-Koutecký, V. Nonadiabatic Dynamics within the Time Dependent Density Functional Theory: Ultrafast Photodynamics in Pyrazine. *Chem. Phys.* **2008**, *349*, 319−324.
(59) Plasser, F.; Crespo-Otero, R.; Pederzoli, M.; Pittner, J.; Lischka, H.; Barbatti, M. Surface Hopping Dynamics with Correlated Single-Reference Methods: 9H-Adenine as a Case Study. *J. Chem. Theory Comput.* **2014**, *10*, 1395−1405.
(60) Gao, X.; Bai, S.; Fazzi, D.; Niehaus, T.; Barbatti, M.; Thiel, W. Evaluation of Spin-Orbit Couplings with Linear-Response Time-Dependent Density Functional Methods. *J. Chem. Theory Comput.* **2017**, *13*, 515−524.
(61) Shu, Y.; Zhang, L.; Chen, X.; Sun, S.; Huang, Y.; Truhlar, D. G. Nonadiabatic Dynamics Algorithms with Only Potential Energies and Gradients: Curvature-Driven Coherent Switching with Decay of Mixing and Curvature-Driven Trajectory Surface Hopping. *J. Chem. Theory Comput.* **2022**, *18*, 1320−1328.
(62) Li, W.; Lucchese, R. R.; Doyuran, A.; Wu, Z.; Loos, H.; Hall, G. E.; Suits, A. G. Superexcited State Dynamics Probed with an Extreme-Ultraviolet Free Electron Laser. *Phys. Rev. Lett.* **2004**, *92*, 083002.
(63) Norman, P.; Dreuw, A. Simulating X-ray Spectroscopies and Calculating Core-Excited States of Molecules. *Chem. Rev.* **2018**, *118*, 7208−7248.
(64) Fabrikant, I. I.; Eden, S.; Mason, N. J.; Fedor, J.Recent Progress in Dissociative Electron Attachment. *Advances In Atomic, Molecular, and Optical Physics*; Arimondo, E., Lin, C. C., Yelin, S. F., Eds.; Academic Press, 2017; Vol. *66*, pp 545−657.
(65) Kossoski, F.; Varella, M. T. d. N. Negative ion states of 5-bromouracil and 5-iodouracil. *Phys. Chem. Chem. Phys.* **2015**, *17*, 17271−17278.
(66) Chenu, A.; Brumer, P. Transform-limited-pulse representation of excitation with natural incoherent light. *J. Chem. Phys.* **2016**, *144*, 044103.
(67) Polli, D.; Altoè, P.; Weingart, O.; Spillane, K. M.; Manzoni, C.; Brida, D.; Tomasello, G.; Orlandi, G.; Kukura, P.; Mathies, R. A.; Garavelli, M.; Cerullo, G. Conical Intersection Dynamics of the Primary Photoisomerization Event in Vision. *Nature* **2010**, *467*, 440−443.
(68) Suchan, J.; Hollas, D.; Curchod, B. F. E.; Slavíček, P. On the importance of initial conditions for excited-state dynamics. *Faraday Discuss.* **2018**, *212*, 307.
(69) Barbatti, M.; Sen, K. Effects of Different Initial Condition Samplings on Photodynamics and Spectrum of Pyrrole. *Int. J. Quantum Chem.* **2016**, *116*, 762−771.
(70) Ruckenbauer, M.; Barbatti, M.; Müller, T.; Lischka, H. Nonadiabatic Excited-State Dynamics with Hybrid ab Initio Quantum-Mechanical/Molecular-Mechanical Methods: Solvation of the Pentadieniminium Cation in Apolar Media. *J. Phys. Chem. A* **2010**, *114*, 6757−6765.
(71) Sellner, B.; Barbatti, M.; Lischka, H. Dynamics starting at a conical intersection: application to the photochemistry of pyrrole. *J. Chem. Phys.* **2009**, *131*, 024312.
(72) Crespo-Otero, R.; Barbatti, M. Spectrum Simulation and Decomposition with Nuclear Ensemble: Formal Derivation and Application to Benzene, Furan and 2-Phenylfuran. *Theor. Chem. Acc.* **2012**, *131*, 1237.
(73) Sršeň, Š.; Slavíček, P. Optimal Representation of the Nuclear Ensemble: Application to Electronic Spectroscopy. *J. Chem. Theory Comput.* **2021**, *17*, 6395−6404.
(74) Hillery, M.; O'Connell, R. F.; Scully, M. O.; Wigner, E. P. Distribution functions in physics: Fundamentals. *Phys. Rep.* **1984**, *106*, 121−167.
(75) Case, W. B. Wigner Functions and Weyl Transforms for Pedestrians. *Am. J. Phys.* **2008**, *76*, 937−946.
(76) Yao, Y.; Hase, W. L.; Granucci, G.; Persico, M. Sampling initial positions and momenta for nuclear trajectories from quantum mechanical distributions. *J. Chem. Phys.* **2021**, *154*, 074115.
(77) Kossoski, F.; Barbatti, M. Nuclear Ensemble Approach with Importance Sampling. *J. Chem. Theory Comput.* **2018**, *14*, 3173−3183.
(78) Kossoski, F.; Varella, M. T. d. N.; Barbatti, M. On-the-fly dynamics simulations of transient anions. *J. Chem. Phys.* **2019**, *151*, 224104.
(79) Lee, H.-W. Wigner trajectories of a Gaussian wave packet perturbed by a weak potential. *Found. Phys.* **1992**, *22*, 995−1010.
(80) Hilborn, R. C. Einstein coefficients; Cross-Sections, *f* Values, Dipole-Moments, and All That. *Am. J. Phys.* **1982**, *50*, 982−986.
(81) Demchenko, A. P.; Tomin, V. I.; Chou, P.-T. Breaking the Kasha Rule for More Efficient Photochemistry. *Chem. Rev.* **2017**, *117*, 13353−13381.
(82) Peng, Q.; Niu, Y.; Shi, Q.; Gao, X.; Shuai, Z. Correlation Function Formalism for Triplet Excited State Decay: Combined Spin−Orbit and Nonadiabatic Couplings. *J. Chem. Theory Comput.* **2013**, *9*, 1132−1143.
(83) Parson, W. W.*Modern Optical Spectroscopy*; Springer-Verlag: Berlin Heidelberg, 2007.
(84) Arbelo-González, W.; Crespo-Otero, R.; Barbatti, M. Steady and Time-Resolved Photoelectron Spectra Based on Nuclear Ensembles. *J. Chem. Theory Comput.* **2016**, *12*, 5037−5049.

(85) Lischka, H.; Nachtigallová, D.; Aquino, A. J. A.; Szalay, P. G.; Plasser, F.; Machado, F. B. C.; Barbatti, M. Multireference Approaches for Excited States of Molecules. *Chem. Rev.* **2018**, *118*, 7293−7361.
(86) Dallos, M.; Lischka, H.; Shepard, R.; Yarkony, D. R.; Szalay, P. G. Analytic Evaluation of Nonadiabatic Coupling Terms at the MR-CI Level. II. Minima on the Crossing Seam: Formaldehyde and the Photodimerization of Ethylene. *J. Chem. Phys.* **2004**, *120*, 7330−7339.
(87) Shiozaki, T.; Győrffy, W.; Celani, P.; Werner, H.-J. Communication: Extended multi-state complete active space second-order perturbation theory: Energy and nuclear gradients. *J. Chem. Phys.* **2011**, *135*, 081106.
(88) Granucci, G.; Toniolo, A. Molecular Gradients for Semiempirical CI Wavefunctions with Floating Occupation Molecular Orbitals. *Chem. Phys. Lett.* **2000**, *325*, 79−85.
(89) Koslowski, A.; Beck, M. E.; Thiel, W. Implementation of a General Multireference Configuration Interaction Procedure with Analytic Gradients in a Semiempirical Context Using the Graphical Unitary Group Approach. *J. Comput. Chem.* **2003**, *24*, 714−726.
(90) Dreuw, A.; Wormit, M. The Algebraic Diagrammatic Construction Scheme for the Polarization Propagator for the Calculation of Excited States. *Wiley Interdiscip. Rev. Comput. Mol. Sci.* **2015**, *5*, 82−95.
(91) Huix-Rotllant, M.; Ferré, N.; Barbatti, M.Time-Dependent Density Functional Theory: from the Fundamentals to Nonadiabatic Dynamics. In *Quantum Chemistry and Dynamics of Excited States: Methods and Applications*; González, L., Lindh, R., Eds.; John Wiley & Sons, 2020; pp 15−46.
(92) Kranz, J. J.; Elstner, M.; Aradi, B.; Frauenheim, T.; Lutsker, V.; Garcia, A. D.; Niehaus, T. A. Time-Dependent Extension of the Long-Range Corrected Density Functional Based Tight-Binding Method. *J. Chem. Theory Comput.* **2017**, *13*, 1737−1747.
(93) Polyak, I.; Hutton, L.; Crespo-Otero, R.; Barbatti, M.; Knowles, P. J. Ultrafast Photoinduced Dynamics of 1,3-Cyclohexadiene Using XMS-CASPT2 Surface Hopping. *J. Chem. Theory Comput.* **2019**, *15*, 3929−3940.
(94) Stojanović, L.; Aziz, S. G.; Hilal, R. H.; Plasser, F.; Niehaus, T. A.; Barbatti, M. Nonadiabatic Dynamics of Cycloparaphenylenes with TD-DFTB Surface Hopping. *J. Chem. Theory Comput.* **2017**, *13*, 5846−5860.
(95) Lischka, H.; Müller, T.; Szalay, P. G.; Shavitt, I.; Pitzer, R. M.; Shepard, R. COLUMBUS − A Program System for Advanced Multireference Theory Calculations. *Wiley Interdiscip. Rev. Comput. Mol. Sci.* **2011**, *1*, 191−199.
(96) Vlaisavljevich, B.; Shiozaki, T. Nuclear Energy Gradients for Internally Contracted Complete Active Space Second-Order Perturbation Theory: Multistate Extensions. *J. Chem. Theory Comput.* **2016**, *12*, 3781−3787.
(97) Barca, G. M. J.; Bertoni, C.; Carrington, L.; Datta, D.; De Silva, N. D.; Deustua, J. E.; Fedorov, D. G.; Gour, J. R.; Gunina, A. O.; Guidez, E.; Harville, T.; Irle, S.; Ivanic, J.; Kowalski, K.; Leang, S. S.; Li, H.; Li, W.; Lutz, J. J.; Magoulas, I.; Mato, J.; Mironov, V.; Nakata, H.; Pham, B. Q.; Piecuch, P.; Poole, D.; Pruitt, S. R.; Rendell, A. P.; Roskop, L. B.; Ruedenberg, K.; Sattasathuchana, T.; Schmidt, M. W.; Shen, J.; Slipchenko, L.; Sosonkina, M.; Sundriyal, V.; Tiwari, A.; Galvez Vallejo, J. L. G.; Westheimer, B.; Włoch, M.; Xu, P.; Zahariev, F.; Gordon, M. S. Recent developments in the general atomic and molecular electronic structure system. *J. Chem. Phys.* **2020**, *152*, 154102.
(98) Balasubramani, S. G.; Chen, G. P.; Coriani, S.; Diedenhofen, M.; Frank, M. S.; Franzke, Y. J.; Furche, F.; Grotjahn, R.; Harding, M. E.; Hättig, C.; Hellweg, A.; Helmich-Paris, B.; Holzer, C.; Huniar, U.; Kaupp, M.; Marefat Khah, A. M.; Karbalaei Khani, S. K.; Müller, T.; Mack, F.; Nguyen, B. D.; Parker, S. M.; Perlt, E.; Rappoport, D.; Reiter, K.; Roy, S.; Rückert, M.; Schmitz, G.; Sierka, M.; Tapavicza, E.; Tew, D. P.; van Wüllen, C. v.; Voora, V. K.; Weigend, F.; Wodyński, A.; Yu, J. M. TURBOMOLE: Modular program suite for ab initio quantum-chemical and condensed-matter simulations. *J. Chem. Phys.* **2020**, *152*, 184107.
(99) Frisch, M. J.; Trucks, G. W.; Schlegel, H. B.; Scuseria, G. E.; Robb, M. A.; Cheeseman, J. R.; Scalmani, G.; Barone, V.; Petersson, G. A.; Nakatsuji, H.; Li, X.; Caricato, M.; Marenich, A. V.; Bloino, J.; Janesko, B. G.; Gomperts, R.; Mennucci, B.; Hratchian, H. P.; Ortiz, J. V.; Izmaylov, A. F.; Sonnenberg, J. L.; Williams; Ding, F.; Lipparini, F.; Egidi, F.; Goings, J.; Peng, B.; Petrone, A.; Henderson, T.; Ranasinghe, D.; Zakrzewski, V. G.; Gao, J.; Rega, N.; Zheng, G.; Liang, W.; Hada, M.; Ehara, M.; Toyota, K.; Fukuda, R.; Hasegawa, J.; Ishida, M.; Nakajima, T.; Honda, Y.; Kitao, O.; Nakai, H.; Vreven, T.; Throssell, K.; Montgomery, J. A., Jr.; Peralta, J. E.; Ogliaro, F.; Bearpark, M. J.; Heyd, J. J.; Brothers, E. N.; Kudin, K. N.; Staroverov, V. N.; Keith, T. A.; Kobayashi, R.; Normand, J.; Raghavachari, K.; Rendell, A. P.; Burant, J. C.; Iyengar, S. S.; Tomasi, J.; Cossi, M.; Millam, J. M.; Klene, M.; Adamo, C.; Cammi, R.; Ochterski, J. W.; Martin, R. L.; Morokuma, K.; Farkas, O.; Foresman, J. B.; Fox, D. J.*Gaussian 16*; Rev. C.01: Wallingford, CT, 2016. https://gaussian.com.
(100) Hourahine, B.; Aradi, B.; Blum, V.; Bonafé, F.; Buccheri, A.; Camacho, C.; Cevallos, C.; Deshaye, M. Y.; Dumitrică, T.; Dominguez, A.; Ehlert, S.; Elstner, M.; van der Heide, T.; Hermann, J.; Irle, S.; Kranz, J. J.; Köhler, C.; Kowalczyk, T.; Kubař, T.; Lee, I. S.; Lutsker, V.; Maurer, R. J.; Min, S. K.; Mitchell, I.; Negre, C.; Niehaus, T. A.; Niklasson, A. M. N.; Page, A. J.; Pecchia, A.; Penazzi, G.; Persson, M. P.; Řezáč, J.; Sánchez, C. G.; Sternberg, M.; Stöhr, M.; Stuckenberg, F.; Tkatchenko, A.; Yu, V. W. z.; Frauenheim, T. DFTB+, a software package for efficient approximate density functional theory based atomistic simulations. *J. Chem. Phys.* **2020**, *152*, 124101.
(101) Dral, P. O.; Ge, F.; Xue, B.-X.; Hou, Y.-F.; Pinheiro, M.; Huang, J.; Barbatti, M. MLatom 2: An Integrative Platform for Atomistic Machine Learning. *Top. Curr. Chem.* **2021**, *379*, 27.
(102) Rackers, J. A.; Wang, Z.; Lu, C.; Laury, M. L.; Lagardère, L.; Schnieders, M. J.; Piquemal, J.-P.; Ren, P.; Ponder, J. W. Tinker 8: Software Tools for Molecular Design. *J. Chem. Theory Comput.* **2018**, *14*, 5273−5289.
(103) Nikitin, E. E. The Theory of Nonadiabatic Transitions: Recent Development with Exponential Models. *Adv. Quantum Chem.* **1970**, *5*, 135−184.
(104) Leggett, A. J.; Chakravarty, S.; Dorsey, A. T.; Fisher, M. P. A.; Garg, A.; Zwerger, W. Dynamics of the dissipative two-state system. *Rev. Mod. Phys.* **1987**, *59*, 1−85.
(105) Grimme, S.; Waletzke, M. A Combination of Kohn-Sham Density Functional Theory and Multi-Reference Configuration Interaction Methods. *J. Chem. Phys.* **1999**, *111*, 5645−5655.
(106) Marian, C. M.; Heil, A.; Kleinschmidt, M. The DFT/MRCI method. *Wiley Interdiscip. Rev. Comput. Mol. Sci.* **2019**, *9*, No. e1394.
(107) Gozem, S.; Gunina, A. O.; Ichino, T.; Osborn, D. L.; Stanton, J. F.; Krylov, A. I. Photoelectron Wave Function in Photoionization: Plane Wave or Coulomb Wave? *J. Phys. Chem. Lett.* **2015**, *6*, 4532−4540.
(108) Plasser, F. TheoDORE A toolbox for a detailed and automated analysis of electronic excited state computations. *J. Chem. Phys.* **2020**, *152*, 084108.
(109) Plasser, F.; Lischka, H. Analysis of Excitonic and Charge Transfer Interactions from Quantum Chemical Calculations. *J. Chem. Theory Comput.* **2012**, *8*, 2777−2789.
(110) Weingart, O. Combined Quantum and Molecular Mechanics (QM/MM) Approaches to Simulate Ultrafast Photodynamics in Biological Systems. *Curr. Org. Chem.* **2017**, *21*, 586−601.
(111) Ren, P. Y.; Ponder, J. W. Polarizable atomic multipole water model for molecular mechanics simulation. *J. Phys. Chem. B* **2003**, *107*, 5933−5947.
(112) Bondanza, M.; Nottoli, M.; Cupellini, L.; Lipparini, F.; Mennucci, B. Polarizable embedding QM/MM: the future gold standard for complex (bio)systems? *Phys. Chem. Chem. Phys.* **2020**, *22*, 14433−14448.
(113) Loco, D.; Lagardère, L.; Cisneros, G. A.; Scalmani, G.; Frisch, M.; Lipparini, F.; Mennucci, B.; Piquemal, J.-P. Towards large scale

hybrid QM/MM dynamics of complex systems with advanced point dipole polarizable embeddings. *Chem. Sci.* **2019**, *10*, 7200−7211.
(114) Bondanza, M.; Demoulin, B.; Lipparini, F.; Barbatti, M.; Mennucci, B. Trajectory Surface Hopping for a Polarizable Embedding QM/MM Formulation. *J. Phys. Chem. A* **2022**, *126*, 6780−6789.
(115) Xue, B.-X.; Barbatti, M.; Dral, P. O. Machine Learning for Absorption Cross Sections. *J. Phys. Chem. A* **2020**, *124*, 7199−7210.
(116) Westermayr, J.; Marquetand, P. Machine Learning for Electronically Excited States of Molecules. *Chem. Rev.* **2020**, *121*, 9873−9926.
(117) Dral, P. O.; Barbatti, M. Molecular excited states through a machine learning lens. *Nat. Rev. Chem.* **2021**, *5*, 388−405.
(118) Pinheiro, M.; Ge, F.; Ferré, N.; Dral, P. O.; Barbatti, M. Choosing the right molecular machine learning potential. *Chem. Sci.* **2021**, *12*, 14396−14413.
(119) Axelrod, S.; Shakhnovich, E.; Gómez-Bombarelli, R. Excited state non-adiabatic dynamics of large photoswitchable molecules using a chemically transferable machine learning potential. *Nat. Commun.* **2022**, *13*, 3440.
(120) Dral, P. O.; Barbatti, M.; Thiel, W. Nonadiabatic Excited-State Dynamics with Machine Learning. *J. Phys. Chem. Lett.* **2018**, *9*, 5660−5663.
(121) Brown, W. M.; Martin, S.; Pollock, S. N.; Coutsias, E. A.; Watson, J.-P. Algorithmic dimensionality reduction for molecular structure analysis. *J. Chem. Phys.* **2008**, *129*, 064118.
(122) Li, X.; Xie, Y.; Hu, D.; Lan, Z. Analysis of the Geometrical Evolution in On-the-Fly Surface-Hopping Nonadiabatic Dynamics with Machine Learning Dimensionality Reduction Approaches: Classical Multidimensional Scaling and Isometric Mapping. *J. Chem. Theory Comput.* **2017**, *13*, 4611−4623.
(123) Glielmo, A.; Husic, B. E.; Rodriguez, A.; Clementi, C.; Noé, F.; Laio, A. Unsupervised Learning Methods for Molecular Simulation Data. *Chem. Rev.* **2021**, *121*, 9722−9758.
(124) Mukherjee, S.; Pinheiro, M., Jr.; Demoulin, B.; Barbatti, M. Simulations of molecular photodynamics in long timescales. *Philos. Trans. R. Soc., A* **2022**, *380*, 20200382.
(125) de Buyl, P.; Colberg, P. H.; Höfling, F. H5MD A structured, efficient, and portable file format for molecular data. *Comput. Phys. Commun.* **2014**, *185*, 1546−1553.
(126) Thompson, A. P.; Aktulga, H. M.; Berger, R.; Bolintineanu, D. S.; Brown, W. M.; Crozier, P. S.; in 't Veld, P. J.; Kohlmeyer, A.; Moore, S. G.; Nguyen, T. D.; Shan, R.; Stevens, M. J.; Tranchida, J.; Trott, C.; Plimpton, S. J. LAMMPS - a flexible simulation tool for particle-based materials modeling at the atomic, meso, and continuum scales. *Comput. Phys. Commun.* **2022**, *271*, 108171.
(127) Fdez Galván, I.; Vacher, M.; Alavi, A.; Angeli, C.; Aquilante, F.; Autschbach, J.; Bao, J. J.; Bokarev, S. I.; Bogdanov, N. A.; Carlson, R. K.; Chibotaru, L. F.; Creutzberg, J.; Dattani, N.; Delcey, M. G.; Dong, S. S.; Dreuw, A.; Freitag, L.; Frutos, L. M.; Gagliardi, L.; Gendron, F.; Giussani, A.; González, L.; Grell, G.; Guo, M.; Hoyer, C. E.; Johansson, M.; Keller, S.; Knecht, S.; Kovačević, G.; Källman, E.; Li Manni, G.; Lundberg, M.; Ma, Y.; Mai, S.; Malhado, J. P.; Malmqvist, P. Å.; Marquetand, P.; Mewes, S. A.; Norell, J.; Olivucci, M.; Oppel, M.; Phung, Q. M.; Pierloot, K.; Plasser, F.; Reiher, M.; Sand, A. M.; Schapiro, I.; Sharma, P.; Stein, C. J.; Sørensen, L. K.; Truhlar, D. G.; Ugandi, M.; Ungur, L.; Valentini, A.; Vancoillie, S.; Veryazov, V.; Weser, O.; Wesołowski, T. A.; Widmark, P.-O.; Wouters, S.; Zech, A.; Zobel, J. P.; Lindh, R. OpenMolcas From Source Code to Insight. *J. Chem. Theory Comput.* **2019**, *15*, 5925−5964.
(128) Humphrey, W.; Dalke, A.; Schulten, K. VMD: Visual molecular dynamics. *J. Mol. Graph.* **1996**, *14*, 33−38.

https://doi.org/10.1021/acs.jctc.2c00804
J. Chem. Theory Comput. 2022, 18, 6851−6865